

Field enhanced photoemission: A new technique for the direct determination of the quasi-free electron energy in dense fluids

Yevgeniy Lushtak^a, C. M. Evans^{a,*}, and G. L. Findley^{a,b}

^a*Department of Chemistry and Biochemistry, Queens College – CUNY, Flushing,
NY 11367 and Department of Chemistry, Graduate Center – CUNY, New York,
NY 10016*

^b*Department of Chemistry, University of Louisiana at Monroe, Monroe, LA 71209*

Abstract

Previous experimental studies of the quasi-free electron energy $V_0(\rho)$ in dense fluids either directly measured $V_0(\rho)$, using photoemission from an electrode immersed in the fluid, or extracted $V_0(\rho)$ from field ionization of a dopant dissolved in the fluid. In this letter, we present a new method to determine directly $V_0(\rho)$, namely field enhanced photoemission. We show that this new method yields data comparable to those obtained from dopant field ionization, thereby making this method superior to direct photoemission studies. Moreover, unlike dopant field ionization, field enhanced photoemission is not limited by the solubility of a dopant in the fluid of interest.

Key words: local Wigner-Seitz model, field enhanced photoemission, quasi-free electron energy

1 Introduction

The creation of low kinetic energy electrons constitutes a dominant energy loss mechanism for high energy photons and particles. The interaction of low energy electrons with dense gases and fluids is, therefore, a crucial problem in radiation chemistry. The study of the quasi-free electron energy $V_0(\rho)$ in dense atomic and molecular fluids has yielded valuable insight into the mobility of electrons in these fluids [1–3], although the relationship between $V_0(\rho)$ and electron mobility in dense fluids is still not well understood. We recently showed that $V_0(\rho)$ exhibits a dramatic increase near the critical density near the critical isotherm in attractive and repulsive atomic fluids [4–9], as well as in attractive molecular fluids [10]. (Attractive and repulsive fluids are defined, respectively, as those with negative and positive zero kinetic energy electron scattering lengths.) $V_0(\rho)$ has been measured directly using photoemission from a metal electrode immersed in the fluid [1, 2, 12–19] or extracted from dopant field ionization spectra [4–9, 11, 12, 20]. However, accurately determining $V_0(\rho)$ in a wide range of fluids is fraught with difficulty.

In a direct measurement $V_0(\rho)$ is the difference between the work function $\phi(\rho)$ in a fluid of density ρ and that in a vacuum (i.e., $\phi(0) \equiv \phi_0$), or

$$V_0(\rho) = \phi(\rho) - \phi_0 . \tag{1}$$

* Corresponding author.

Email addresses: cherice.evans@qc.cuny.edu (C. M. Evans),
findley@ulm.edu (G. L. Findley).

In previous studies [1, 2, 12–19] the work function was determined using the photoelectric effect on an electrode immersed in the fluid. The current i from a photoemitting electrode in a vacuum is given by [14, 21]

$$i \propto A k^2 T^2 F(x) \quad (2)$$

where A is an unknown temperature and frequency independent constant that depends on the potential step x_0 at the electrode boundary as well as on the fraction of electrons that can absorb a photon and escape; T is the temperature of the system; and $x = [h\nu - \phi(\rho)]/kT$, with $h\nu$ being the photon energy and k being Boltzmann's constant. $F(x)$ in eq. (2) is Fowler's function, or

$$\frac{1}{2}x^2 + \frac{1}{6}\pi^2 - e^{-x} + \frac{1}{2^2}e^{-2x} - \frac{1}{3^2}e^{-3x} \dots, \quad (3)$$

when $x \geq 0$. To make eq. (2) more applicable to experimental data, it is usually rewritten as [1, 14, 21]

$$\ln\left(\frac{i}{k^2 T^2}\right) = \ln A + \ln\left[f(x) + \frac{1}{2}x^2\right] \quad (4)$$

where $f(x) = \pi^2/6 - e^{-x} \dots \approx 0$ when sufficiently close to threshold. However, while not readily apparent from eq. (4), the parameters A , $f(x)$ and $\phi(\rho)$ are strongly coupled. Thus, the work function $\phi(\rho)$ is very sensitive to the initial guess for all three unknown parameters in a nonlinear least squares analysis of the photoemission data to eq. (4). Moreover, the assumption that the potential step x_0 at the electrode boundary remains constant when the electrode is immersed in the dense fluid is not valid, since the fluid will form a surface layer on the electrode as well as impede electrons moving to the detector through multiple scattering events. The sensitivity to initial guesses during analysis of the data, as well as the invalid assumptions, yield data sets with very high scatter (cf. Fig. 1a, for example), making any investigation of

small effects on $V_0(\rho)$ (such as a critical point effect) impossible.

On the other hand, the indirect determination of $V_0(\rho)$ utilizes a dopant molecule dissolved into the perturbing fluid. High- n dopant Rydberg states converging to the first ionization energy are excited using vacuum ultraviolet radiation, and are field ionized with a DC field. The perturber influenced dopant ionization energy $I(\rho)$ is determined by taking the difference between two photoionization spectra measured with different applied electric fields (after intensity normalizing the spectra to remove the effects of secondary ionization). This difference yields a peak which represents dopant Rydberg states ionized by the high field but not the low field. Plotting the energy position of this field ionization peak as a function of the sum of the square roots of each field and then extrapolating to zero field gives the ionization energy of the dopant in the presence of the perturber, but in the absence of an electric field. Once $I(\rho)$ is determined, $V_0(\rho)$ is extracted via [8, 10–12, 20]

$$V_0(\rho) = I(\rho) - I_g - P_+(\rho) , \quad (5)$$

where I_g is the ionization energy of the neat gaseous dopant and $P_+(\rho)$ is the ensemble averaged dopant cationic core/perturber polarization energy. While I_g can be experimentally measured, $P_+(\rho)$ must be theoretically determined. Calculating $P_+(\rho)$ within a standard statistical mechanical model with appropriate choices for the dopant/perturber intermolecular potential yields quasi-free electron energies $V_0(\rho)$ that are comparable to those directly evaluated, but with significantly less scatter (cf. Fig. 1b, for example). This lower scatter allowed for the observation of a striking critical point effect in various atomic [4–9] and molecular fluids [10] which, in turn, led to the development of the new, more accurate local Wigner-Seitz model [10, 11] for $V_0(\rho)$. However,

this technique is limited by the requirement that the dopant be soluble in the fluid of interest, and by the fact that the dopant must ionize in an energy region where the fluid is transparent. Thus, an investigation of critical point effects on $V_0(\rho)$ in repulsive fluids (which have very low critical temperatures) or in most molecular fluids cannot be achieved using dopant field ionization.

In this paper we present a new technique for directly measuring the quasi-free electron energy, namely field enhanced photoemission. In this technique, we extract the work function $\phi(\rho)$ by using the difference between two photoemission spectra taken at different electric field strengths. The field enhanced photoemission (FEP) signal is the photon energy plotted as a function of this difference. We show that, when the FEP signal is appropriately corrected for the applied electric fields, it possesses a linear region above the photoemission threshold. This linear region is then fitted using a linear least squares analysis to give an energy intercept that is related to the work function $\phi(\rho)$. We then use $\phi(\rho)$ to determine $V_0(\rho)$ through eq. (1) and illustrate that one obtains comparable results to those from dopant field ionization. For this study, Ar was chosen as the perturber because of the substantial body of $V_0(\rho)$ data (cf. Fig. 1) obtained from photoemission as well as dopant field ionization.

2 Experimental

Photoemission spectra from a Pt electrode were measured with monochromatic vacuum ultraviolet synchrotron radiation [20] using the stainless steel Seya-Namioka beamline equipped with a high energy (5 - 35 eV) grating at the University of Wisconsin Synchrotron Radiation Center. The radiation, having a resolution of ~ 10 meV in the spectral region of interest, enters a copper

sample cell (cf. Fig. 2) capable of withstanding 100 bar. The cell is fitted with a MgF_2 or LiF window that possesses a 10 nm thick strip of sputter deposited Pt along the diameter to act as the photoemitting electrode. (A thicker deposit of Pt or silver epoxy is used at the end of the strip to ensure good electrical contact.) A stainless steel electrode is attached to the window perpendicular to the platinum strip. The electrode spacing is 0.1 cm. The electric field was applied using a positive voltage on the stainless steel electrode, while the signal was measured from the Pt electrode using a Keithley 486 picoammeter. The cell was attached to an open cycle liquid nitrogen cryostat and resistive heater that can maintain the cell temperature to ± 0.5 K.

Argon (Matheson Gas Products, 99.9999%) was used without further purification. Prior to the introduction of Ar, the gas handling system was baked to a base pressure of low 10^{-8} Torr. The flux from the Seya beamline was measured using a GaAsP diode placed in front of the sample cell and was monitored during individual photoemission spectrum using a Ni mesh intersecting the beam before the sample cell. All photoemission spectra were normalized to monochromator flux using the GaAsP diode, however, since the Ni mesh also has its photoemission threshold in the energy region of interest. To minimize error induced by perturber/electrode interactions, a series of photoemission spectra were measured with minimal Ar pressure at various voltages for each temperature. Since it requires $\sim 1.4 \times 10^{14}$ Ar atoms to coat the surface of the Pt electrode (under the assumption of a Lennard Jones fluid), these low density spectra were measured with densities greater than 1×10^{19} atoms/cm³ and were used to establish the “zero” density work function ϕ_0 for each isotherm.

3 Field enhanced photoemission: Theory

In the presence of an electric field, Fowler's equations (i.e., eqs. (2) and (4)) for photoemission from a clean electrode in a vacuum change by replacing $x = [h\nu - \phi(\rho)]/kT$ with $x = [h\nu - \phi(\rho) + \sqrt{e^3 E}]/kT$ [22, 23], where e is the electron charge, and E is the electric field. Thus, eq. (2) can be rewritten as [22]

$$i \propto A k^2 T^2 \left[f(x(E)) + \frac{1}{2} \left(\frac{h\nu - \phi_0 + \sqrt{e^3 E}}{kT} \right)^2 \right],$$

which simplifies to

$$i \propto A k^2 T^2 \left[\frac{1}{6} \pi^2 + \frac{1}{2} \left(\frac{h\nu - \phi(\rho) + \sqrt{e^3 E}}{kT} \right)^2 \right] \quad (6)$$

when $(h\nu - \phi(\rho) + \sqrt{e^3 E})/kT \gg 0$.

When the electrode is immersed in a fluid, $A \rightarrow B(T, \rho)$, the perturber interacts with the electrode, which changes the potential step, and the photoemitted electron undergoes multiple scattering events with the perturber, which changes the fraction of electrons that reach the detector. Similarly, the electric field polarizes the fluid, which requires that changes in the dielectric constant as a function of density and temperature also be considered. Under these conditions eq. (6) becomes

$$i \propto B(T, \rho) k^2 T^2 \left[\frac{1}{6} \pi^2 + \frac{1}{2 k^2 T^2} \left(h\nu - \phi(\rho) + \sqrt{\left(\frac{e^3 E}{4\pi \varepsilon(T, \rho)} \right)} \right)^2 \right] \quad (7)$$

where $\varepsilon(T, \rho)$ is the temperature and density dependent dielectric constant.

The difference Δi in photoemission from the perturbed electrode under the

influence of two different electric fields is, therefore,

$$\begin{aligned} \frac{\Delta i}{B(T, \rho)} &\propto \frac{1}{2} \left\{ \left(h\nu - \phi(\rho) + \sqrt{\Lambda_H} \right)^2 - \left(h\nu - \phi(\rho) + \sqrt{\Lambda_L} \right)^2 \right\} \\ &\propto [h\nu - \phi(\rho)] (\sqrt{\Lambda_H} - \sqrt{\Lambda_L}) + \frac{1}{2} (\Lambda_H - \Lambda_L) \end{aligned} \quad (8)$$

under the assumption that $B(T, \rho)$ is field independent, and where $\Lambda_i = e^3 E_i / (4\pi\epsilon(T, \rho))$ with $i = L, H$ for the low and high electric field, respectively.

Considerable rearrangement of eq. (8) gives

$$h\nu \propto b \Delta i_E + a, \quad (9)$$

where the slope is $b = 1/B(T, \rho)$,

$$\Delta i_E \equiv \frac{\Delta i}{\sqrt{\Lambda_H} - \sqrt{\Lambda_L}},$$

and the intercept $a(\rho)$ is

$$a(\rho) = \phi(\rho) - \frac{1}{2} (\sqrt{\Lambda_H} + \sqrt{\Lambda_L}). \quad (10)$$

Thus, the FEP signal, which is a plot of photon energy as a function of Δi_E , should possess a linear region with an intercept that yields the work function $\phi(\rho)$ in the zero field limit.

4 Results and Discussion

Fig. 3 presents representative photoemission spectra of Pt in Ar measured at 158 K at various electric field strengths. Both at low density (i.e., Fig. 3a, for example) and at high density (i.e., Fig. 3b, for example), a distinct enhancement of the photocurrent as a function of electric field is observed. (We should note here that the significant decrease in photocurrent between the low density and high density spectrum is probably caused by multiple

scattering effects changing $B(T, \rho)$.) Similar series of photoemission spectra were obtained for various perturber number densities and at various noncritical temperatures, as well as on an isotherm near the critical isotherm. Electric fields were chosen to maximize the field effect while not creating dielectric breakdown in the cell. Because $\phi(\rho)$ is temperature dependent, a set of four low density field dependent photoemission spectra were measured for each each isotherm, thus providing a “zero” density signal that corrects for these temperature differences. Only a selection of these data sets are shown for brevity.

In order to obtain a field enhanced photoemission signal, however, one must first determine the change in the dielectric constant as a function of temperature and density. Schmidt and Moldover [24] showed that, in the temperature range of 273–323K and at pressures of up to 70 bar, the dielectric permittivity of Ar is temperature independent and can be modeled using

$$\frac{\varepsilon - 1}{\varepsilon + 2} = c_0\rho + c_1\rho^2 ,$$

where $c_0 = 4.14203 \pm 0.00019 \text{ cm}^3/\text{mol}$ and $c_1 = 1.16 \pm 0.06 \text{ cm}^6/\text{mol}^2$. Assuming that the temperature independence is valid out to the density of the triple point liquid implies that the dielectric constant varies from $0.999\bar{7}$ at the lowest density of $0.041 \times 10^{21} \text{ cm}^{-3}$ to $0.820\bar{8}$ at the density of $22.0 \times 10^{21} \text{ cm}^{-3}$, which is near the triple point. Since this change represents a variation of approximately 20% over the entire fluid density range of Ar, neglecting the density dependence of the dielectric constant will yield significant scatter in $\phi(\rho)$ and, subsequently $V_0(\rho)$, as observed in Fig. 1a.

Fig. 4 presents the photon energy as a function of Δi_E for the six possible pairwise differences that can be taken between the spectra shown in Fig. 3, in an

expanded view to highlight the linear portion of the FEP signal. Again, similar FEP spectra exist for a series of data points taken across the density range at noncritical temperatures and on an isotherm near the critical isotherm. Fitting these data with a linear least squares analysis to eq. (9) yields an intercept that is shown in Fig. 5, plotted as a function of $\sqrt{\Lambda_H} + \sqrt{\Lambda_L}$ for the low density (\bullet) and the high density (\blacktriangledown) FEP signals given in Fig. 4a and 4b, respectively. Two additional sets of FEP intercepts are also shown in Fig. 5, namely that for $\rho = 4.1 \times 10^{21} \text{ cm}^{-3}$ and for $\rho = 7.1 \times 10^{21} \text{ cm}^{-3}$, also measured at 158 K. Clearly, the intercepts are linearly dependent on $\sqrt{\Lambda_H} + \sqrt{\Lambda_L}$ and all four data sets yield similar slopes. Extrapolating these data sets back to zero field leads to the determination of the work function $\phi(\rho)$ for each density. Setting $\phi(0.041 \times 10^{21} \text{ cm}^{-3}) = \phi_0$ allows us to determine $V_0(\rho)$ using eq. (1).

Repeating this process for a variety of densities from medium density to the density of the triple point liquid, at noncritical temperatures and on an isotherm near the critical isotherm, allows one to determine the density and temperature dependence of $V_0(\rho)$. These results are shown in Fig. 6 as a function of Ar number density ρ and in comparison to a local Wigner-Seitz calculation optimized to the high precision dopant field ionization data of Fig. 1b. In Fig. 6, each different solid marker represents a different noncritical temperature, while the open markers represent a temperature near the critical temperature of 151 K. At each of these temperatures, a new ϕ_0 was defined by measuring field effects on photoemission with a very low density of Ar present, and with $V_0(\rho)$ being determined using eq. (1) with this new ϕ_0 . Because the temperature dependence of the work function is built into the technique and because the differences between spectra cancel out the imperfections in the sputter coated Pt electrode, the measured $V_0(\rho)$ has a scatter that is com-

parable to that obtained using dopant field ionization measurements. Since measuring accurate, high precision $V_0(\rho)$ can now be accomplished without a dopant, one can begin to investigate the quasi-free electron energy in repulsive atomic and molecular systems (all of which are poor solvents), as well as in highly absorbing molecular fluids. We are currently using this new technique to measure the quasi-free electron energy in He from low density to the triple point density of the liquid, at noncritical temperatures and on an isotherm near the critical isotherm.

5 Acknowledgement

The experimental measurements reported here were performed at the University of Wisconsin Synchrotron Radiation Center (NSF DMR-0537588). This work was supported by grants from the Petroleum Research Fund (45728-B6), from the Professional Staff Congress–City University of New York (62386-0040), and from the National Science Foundation (NSF CHE-0956719).

References

- [1] R. Reininger, U. Asaf, I. T. Steinberger, S. Basak, *Phys. Rev. B* 28 (1983) 4426.
- [2] Richard M. Stratt, *Ann. Rev. Phys. Chem.* 41 (1990) 175, and references therein.
- [3] R. A. Holroyd, W. F. Schmidt, *Ann. Rev. Phys. Chem.* 40 (1989) 439, and references therein.
- [4] C. M. Evans, G. L. Findley, *Chem. Phys. Lett.* 410 (2005) 242.
- [5] C. M. Evans, G. L. Findley, *J. Phys. B: At. Mol. Opt. Phys.* 38 (2005) L269.

- [6] Luxi Li, C. M. Evans, G. L. Findley, *J. Phys. Chem. A* 109 (2005) 10683.
- [7] Xianbo Shi, Luxi Li, C. M. Evans, G. L. Findley, *Chem. Phys. Lett.* 432 (2006) 62.
- [8] Xianbo Shi, Luxi Li, C. M. Evans, G. L. Findley, *Nucl. Inst. Meth. Phys. A* 582 (2007) 270.
- [9] C. M. Evans, Yevgeniy Lushtak, G. L. Findley, *Chem. Phys. Lett.* 501 (2011) 202.
- [10] Xianbo Shi, Luxi Li, G. L. Findley, C. M. Evans, *Chem. Phys. Lett.* 481 (2009) 183.
- [11] C. M. Evans, G. L. Findley, *Phys. Rev. A* 72 (2005) 022717.
- [12] A. K. Al-Omari, Ph.D. dissertation, University of Wisconsin Madison, Madison, WI, 1996, and references therein.
- [13] W. F. Schmidt, E. Illenberger, Eds., *Electronic excitations in liquified rare gases*, Am. Sci. Publ., Valencia, CA, 2005, and references therein.
- [14] R. A. Holroyd, M. Allen, *J. Chem. Phys.* 54 (1971) 5014.
- [15] A. O. Allen, P. J. Kuntz, W. F. Schmidt, *J. Phys. Chem.* 88 (1984) 3718.
- [16] W. Tauchert, H. Jungblut, W. F. Schmidt, *Can. J. Chem.* 55 (1877) 1860.
- [17] A. O. Allen, *Natl. Stand. Ref. Data.* 58 (1976).
- [18] R. A. Holroyd, B. K. Dietrich, H. A. Schwarz, *J. Phys. Chem.* 76 (1972) 3794.
- [19] R. A. Holroyd, S. Tames, A. Kennedy, *J. Phys. Chem.* 79 (1975) 2857.
- [20] Xianbo Shi, Ph.D. dissertation, The Graduate Center – CUNY, 2010, and references therein.
- [21] R. H. Fowler, *Phys. Rev.* 38 (1931) 45.

- [22] E. Guth, C. J. Mullin, *Phys. Rev.* 59 (1941) 867.
- [23] R. H. Fowler, L. Nordheim, *Proc. Roy. Soc. London A* 119 (1928) 173.
- [24] J. W. Schmidt, M. R. Moldover, *Int. J. Thermophys.* 24 (2003) 375.
- [25] P. Marchand, L. Marmet, *Rev. Sci. Inst.* 54 (1983) 1034.

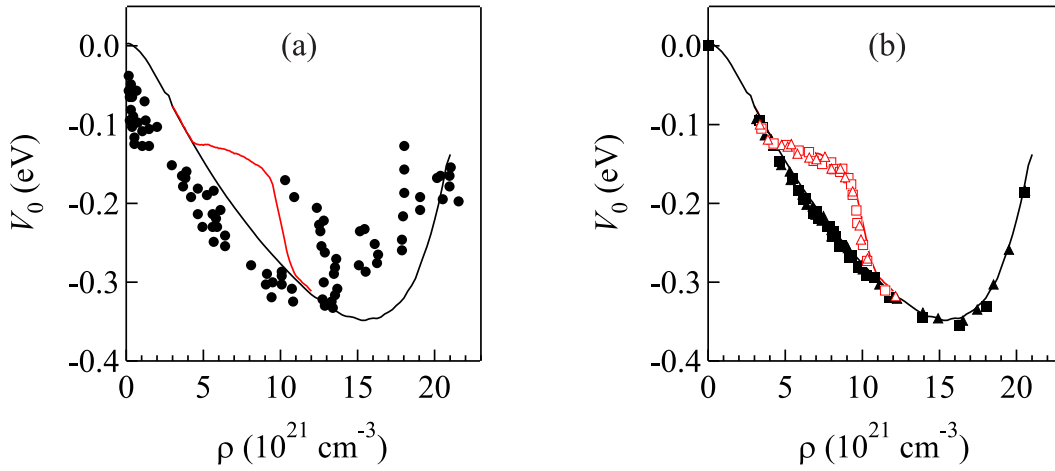


Fig. 1. [Color online] The quasi-free electron energy $V_0(\rho)$ in argon plotted as a function of Ar number density ρ . (a) $V_0(\rho)$ obtained from various photoinjection studies [1, 12, 13] at noncritical temperatures. (b) $V_0(\rho)$ obtained from dopant field ionization using eq. (5) [4, 5, 11], with the solid markers representing noncritical temperatures and the open markers representing critical temperatures. The lines are a local Wigner-Seitz calculation [4, 5, 11] optimized to the data in (b).

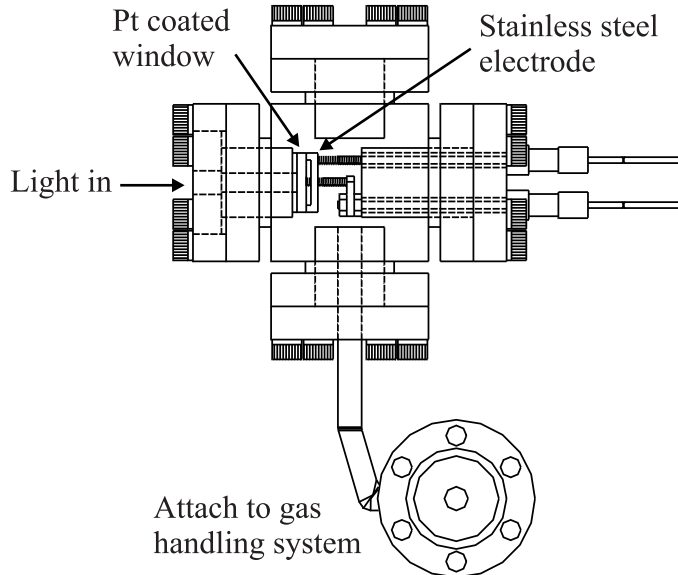


Fig. 2. A schematic of the sample cell used to measure the photoemission spectra necessary for this study.

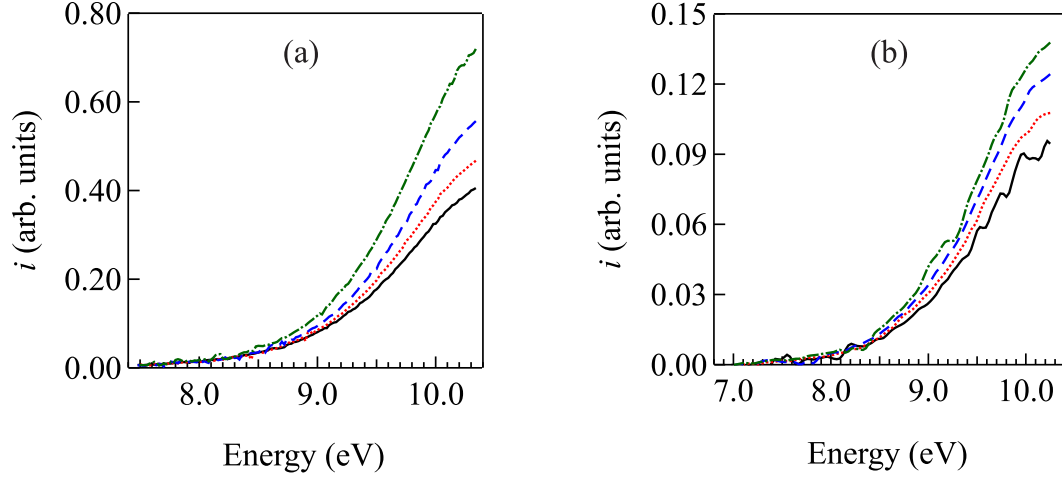


Fig. 3. [Color online] Photocurrent plotted as a function of photon energy for argon number densities of (a) $0.041 \times 10^{21} \text{ cm}^{-3}$ and (b) $11.0 \times 10^{21} \text{ cm}^{-3}$ at a temperature of 158 K. In (a) the applied fields are (—) 2500 V/cm, (\cdots) 5000 V/cm, (— —) 7500 V/cm and (— · —) 10,000 V/cm. In (b) the fields are (—) 20 kV/cm, (\cdots) 25 kV/cm, (— —) 30 kV/cm and (— · —) 35 kV/cm.

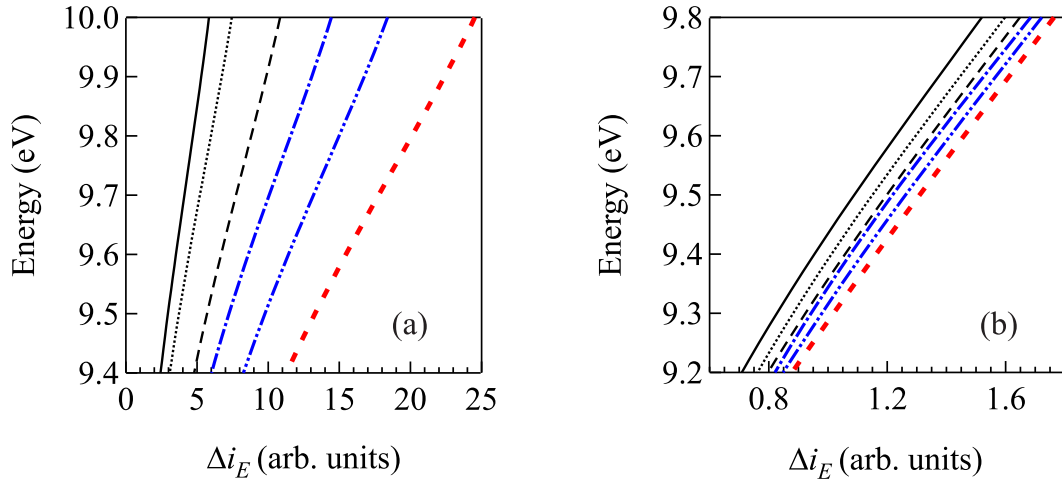


Fig. 4. [Color online] Photon energy plotted as a function of $\Delta i_E(\rho)$ for argon number densities of (a) $0.041 \times 10^{21} \text{ cm}^{-3}$ and (b) $11.0 \times 10^{21} \text{ cm}^{-3}$ at a temperature of 158 K. The lines represent the differences in the spectra presented in Fig. 3 with the lowest set of fields given by (—) and the highest by (— —). Before taking the differences, each photocurrent spectrum was smoothed using a Gaussian smoothing algorithm [25] as implemented in Wavemetrics IgorPro to reduce noise in the differences. See text for discussion.

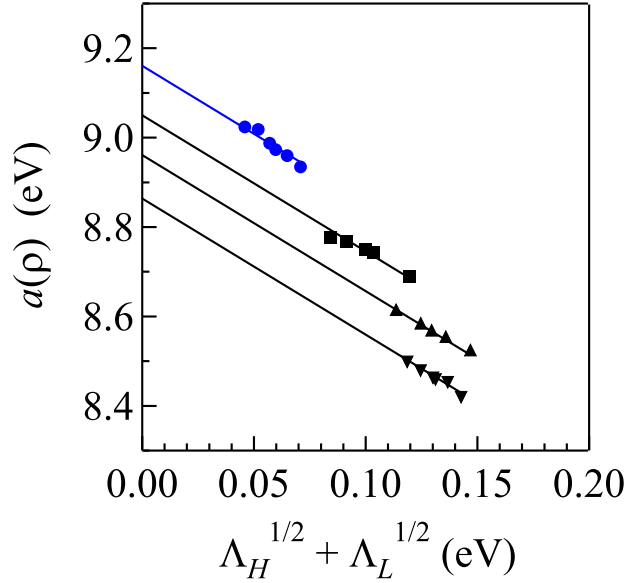


Fig. 5. [Color online] The intercept $a(\rho)$ of representative field enhanced photoemission plots (cf. Fig. 4, for example), measured at 158 K, plotted as a function of $(\sqrt{\Lambda_H} + \sqrt{\Lambda_L})$. The number densities ρ are (●) $0.041 \times 10^{21} \text{ cm}^{-3}$, (■) $4.1 \times 10^{21} \text{ cm}^{-3}$, (▲) $7.1 \times 10^{21} \text{ cm}^{-3}$ and (▼) $11.0 \times 10^{21} \text{ cm}^{-3}$. Each line represents a linear least squares analysis to the data having a slope of -3.04 at this temperature and an intercept of $\phi(\rho)$. See text for discussion.

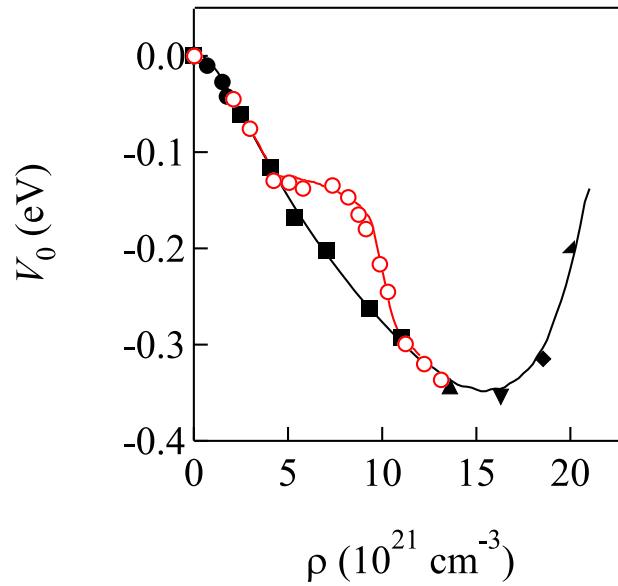


Fig. 6. [Color online] The quasi-free electron energy $V_0(\rho)$ determined from field enhanced photoemission plotted as a function of Ar number density ρ . The solid markers represent various noncritical isotherms, while the open markers represent an isotherm near the critical isotherm of 151 K. The solid lines are a local Wigner-Seitz calculation [4, 5, 11] optimized to the data in Fig. 1b. See text for discussion.